FATIGUE CRACK RESISTANCE OF 6061 AND 7005 ALUMINUM ALLOY – AL_2O_3 PARTICULATE COMPOSITES

L. Collini*, A. Pirondi and D. Fersini

Dept. of Industrial Engineering - University of Parma, Parco Area delle Scienze 181/A, 43100 Parma, Italy

ABSTRACT

In this work the fatigue crack growth (FCG) properties of 6061 and 7005 aluminum alloys reinforced with 20% and 10% alumina particles, respectively, are characterized and compared. Standard FCG tests are conducted in Stage I (near-threshold growth rates) and Stage II (Paris regime) at *R*-ratio 0.1 and 0.5. Both LT and TL crack orientations are considered. The increase of FCG rates with *R*-ratio is interpreted in terms of crack closure for which, in metal matrix composites, contributions from crack surface roughness, crack deflection and particle trapping mechanisms play an important role. The effective stress intensity range at the crack tip, ΔK_{eff}, is estimated in the near-threshold regime applying the traditional Elber's approach and, alternatively, three recently introduced models. The analysis at the SEM microscope of fracture surfaces in correspondence of increasing values of ΔK highlighted crack path features and propagation mechanism.

1. INTRODUCTION

Particle Metal Matrix Composites (PMMCs) are being increasingly considered for several applications in the automotive field (brake discs and drums, brake callipers, pistons), in the railway field (brake discs, callipers and shoes), in sporting goods (bicycle frames, golf clubs and rods), in the aeronautical (reinforced Ti-alloys) and in electronic industries (device substrates, packaging). The interest about PMMCs mainly concerns their lower cost with respect to short or long fibre-reinforced MMCs, [1]. Commonly, Al- or Mg-alloys are the matrix materials while high modulus ceramics, such as Al_2O_3 and SiC, are the reinforcement materials in form of particles. The main improvements given by PMMCs with respect to the matrix alone are higher stiffness, mechanical and wear resistance, with a quasi-isotropic mechanical response, [1, 2].

In addition to the standard mechanical properties such as tensile or fatigue strength, the knowledge of fatigue crack growth (FCG) properties is also important to guarantee reliable in-service durability. At low FCG rates regime, PMMCs show a better performance than unreinforced alloys due to particle-activated shielding mechanisms such as crack deflection or trapping, [3-8]. Furthermore, in cast PMMCs the particles are often located at the grain boundary, leading to a crack tip shielding mechanism known as *egg-shell*, [9].

A great influence on FCG properties comes from the *R*-ratio $R = K_{min}/K_{max}$, where K_{min} and K_{max} are the minimum and maximum values of the applied Stress Intensity Factor (SIF), respectively. As in the unreinforced alloy, higher *R*-ratios lead to higher FCG rates. This has been interpreted in terms of crack closure, [5], which occurs in PMMCs due to crack surface roughness induced by particles or crack bridging, besides plastic wake contribution that is present also in the unreinforced material.

The aim of this work is to characterize the FCG behaviour of 6061 and 7005 in T6 state aluminium alloy, reinforced with 20% and 10% alumina (Al_2O_3) particles respectively. The influence of *R*-ratio on FCG and crack closure mechanism in the near-threshold rate are analysed. The traditional opening load or Elber approach, [11], the *ACR* technique, [12], the $2/\pi$ or partial crack closure model, [13], and a recent double-parameter empirical model, [14], are applied on experimental data to determine and compare the FCG rates in terms of effective SIF, ΔK_{eff}. In the near-threshold and high FCG rate regimes, the role of particle-type reinforcement on crack closure and propagation mechanism is studied through the SEM analysis of fracture surfaces. A graphical estimation of crack profile roughness is made, in order to correlate the applied stress with failure mechanism and crack-particle interaction.

(*) reference author, e-mail: collini@me.unipr.it

2. THEORETICAL BACKGROUND ON CRACK CLOSURE ANALYSIS

2.1 The Elber's approach – ASTM technique

The conventional method proposed by Elber more than 30 years ago, assumes that the SIF corresponding to crack opening (K_{op}) can be directly related to a deviation from the linearity of load vs crack-mouth-displacement curve. The load-displacement plot should conform to a straight line when crack closure is not active. On the other hand, when closure is active, the straight line becomes a non-linear curve due to the progressive contact between the crack faces while unloading, as illustrated in figure 1.

According to Elber's approach the following loading phase will see the crack tip to open only when the load reaches the opening load, P_{op}, thus reducing the ΔK effectively applied at the crack tip to a $\Delta K_{eff} = K_{max} - K_{op}$, where K_{op} is the SIF corresponding to P_{op}, [11]. On the basis of this approach, the ASTM regulation estimates K_{op} as the value that gives a 2% deviation from linearity, [15].

2.2 The ACR technique

Recently, Donald [12] measured significant crack tip straining even below the K_{op} load. A new method to calculate the effective ΔK has been proposed, taking into account the effect of a partially closed crack on the stress field ridistribution at the crack tip. An *adjusted compliance ratio* (*ACR*) is defined as:

$$ACR = \frac{C_s - C_i}{C_0 - C_i} \tag{1}$$

where $C_i = dV_i/dP_i$ (inverse slope of load-strain) is the compliance of the specimen (including the notch, but prior to crack initiation), C_s the secant compliance and the C_0 the compliance calculated above P_{op}, as illustrated in figure 1, [12].

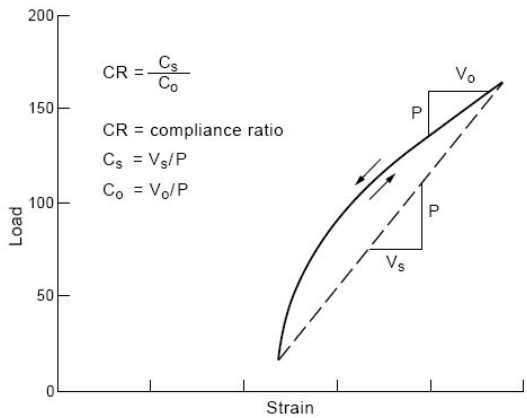

"**Fig. 1.** Load-strain diagram at crack tip showing the compliace ratio technique, [12]"

The effective SIF is obtained simply by multiplying the applied ΔK, by *ACR* parameter:

$$\Delta K_{eff} = ACR \cdot \Delta K \tag{2}$$

2.3 The 2/π physical model

Paris et al. [13] introduced the new concept of partial crack closure, assuming that closure or crack surface interference does not occur at the crack tip. The interference between crack

faces at a small distance behind the crack tip may only partially shield the crack tip from fatigue damage, as schematically shown in figure 2, [13]. Especially at near-threshold FCG, surface roughness, oxide layers or uneven residual stresses in the plastic wave of a propagating crack, are believed to act as an elastic wedge inserted between the crack surfaces.

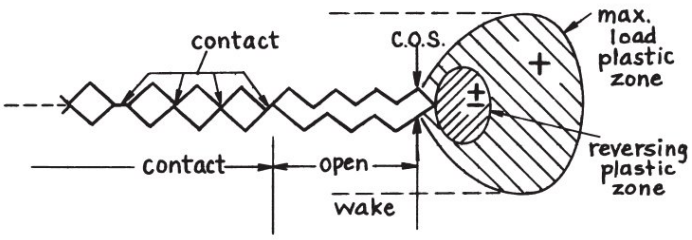

"**Fig. 2.** Physical representation of partial crack closure behind the crack tip, [13]"

Therefore a non-negligible contribution to fatigue damage may take place in the load range below P_{op}. The effective opening load ΔK_{eff} is estimated to be in the range:

$$K_{max} - \frac{2}{\pi} K_{op} - \left(1 - \frac{2}{\pi}\right) K_{min} \leq \Delta K_{eff} \leq K_{max} - \frac{2}{\pi} K_{op} \tag{3}$$

where K_{op} as previously described. Generally the term $(1\text{-}2/\pi)K_{min}$ can be neglected giving $\Delta K_{eff} = K_{max} - \frac{2}{\pi} K_{op}$.

2.4 K_{max} and ΔK^+ parameters

For brittle materials also the maximum stress intensity factor K_{max} is known to play a role and the closure concept is not able to completely justify crack growth behaviour. A new empirical approach has been proposed by Kujawski to assess *R*-ratios effect, [14]: in this approach the mechanical driving force is calculated using solely the positive part ΔK^+ of the applied ΔK and the corresponding maximum value K_{max}:

$$\Delta K = K_{\max}^{\alpha} \Delta K^{+(1-\alpha)} \tag{4}$$

where the so-called *sensitivity* α is a material parameter ranging from 0 for ductile to 1 for brittle materials. For aluminium alloys a value of α equal to 0.5 generally gives a good agreement with the experimental data.

3. METODOLOGIES AND EXPERIMENTAL PROCEDURE

3.1 Material

The composites under testing are 6061 and 7005 aluminum alloy with respectively 20% and 10% vol. of Al_2O_3 particles incorporated by compocasting. The mix is extruded and aged to obtain a bar of 100x7mm^2 cross-section in a T6 state. The tensile mechanical properties given by the manufacturer are reported in Tab. 1. The fracture toughness measured in a previous work, [16], is reported in Tab. 2 for both the LT and TL orientation of crack with respect to the extrusion direction.

"**Table 1.** Mechanical properties of the composites."

Material	E (GPa)	R_y (MPa)	R_m (MPa)	A_f%
AA6061/Al_2O_3/20p	97.2	360	375	4
AA7005/ Al_2O_3/10p	84.0	345	395	7

"**Table 2.** Fracture toughness of the composites, [16]"

Direction	K_{IC} (MPa $\sqrt{m}$)	
	AA6061	AA7005
LT	16.21	19.40
TL	15.38	17.51

The micrographs of Fig. 3 show the high uniformity of particle distribution of both the materials, where only a few isolated large particles and clusters are visible. The particle characteristics have been analysed with the help of a commercial software. Results are summarized in Tab. 3, where D_C and D_f indicate a circle area-equivalent diameter and Feret diameter of particles. The average equivalent diamater D_C is around 4 microns in both 6061 and 7005 alloys, the particles number per mm^2 reflects the volume content of reinforcement.

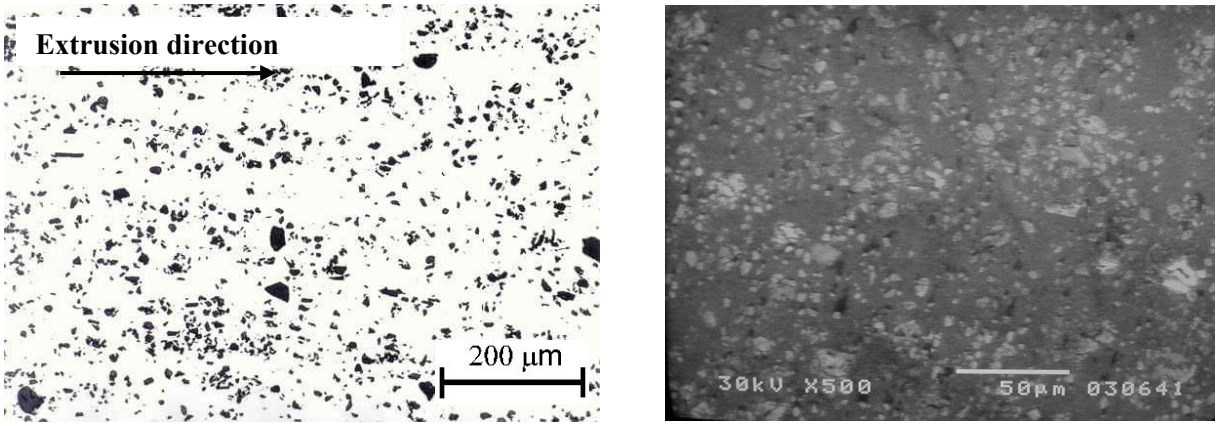

(a) (b)

"**Fig. 3.** Microstructures of (a) AA6061/Al_2O_3/20p and (b) AA7005/Al_2O_3/10p alloys"

"**Table 3.** Particle features in the PMMCs"

Material	D_{cmax} (μm)	D_{cavg} (μm)	D_{fmax} (μm)	D_{favg} (μm)	Particle number (1/mm^2)
AA6061/Al_2O_3/20p	23.2	4.2	53.1	7.2	2440
AA7005/Al_2O_3/10p	38.8	3.6	74.5	4.2	1456

3.2 Specimen and crack length monitoring

Mini-CT specimen as depicted in figure 4 with length W = 24mm and thickness B = 7mm were adopted during the experimental activity. The applied load was controlled by means of 3000N load cell in order to ensure adequate sensitivity and precision.

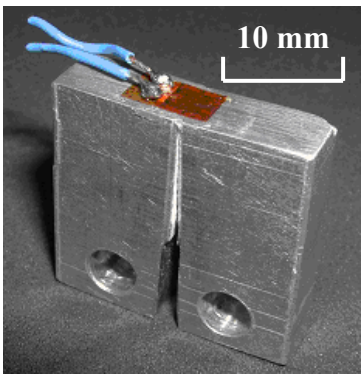

"**Fig. 4.** Mini-CT specimen"

The crack length was monitored during the test with the back-face strain-gage (BFSG) technique, because of the small dimensions of the specimen. In this technique, a strain gage is glued to the back face of the specimen and a compliance C is determined from the back-face strain (ε) and load (P) data as:

$$C = \frac{-\varepsilon W}{P} \tag{5}$$

The crack length ratio a/W is expressed in by a classical polynomial relationship:

$$\frac{a}{W} = a_0 + a_1 u + a_2 u^2 + a_3 u^3 + a_4 u^4 + a_5 u^5 \tag{6}$$

as a function of

$$u = \frac{1}{1 + \sqrt{BEC}} \tag{7}$$

The coefficients $a_0, \ldots, a_5$ were calibrated by Finite Element Analysis and the results are in good agreement with previous results obtained with the surface replication technique, with influence function method and from the literature, [17].

3.3 Test method and evaluation of ΔK_{th}

Constant load amplitude test were conducted to investigate the steady-state propagation regime, while continuous load-shedding procedure with exponential decay of ΔK according to [15] was adopted to investigate the near-threshold regime. All of the tests were performed at a frequency of 10 Hz in lab air. The FCG data are presented in log-log (da/dN-ΔK) plots. Crack propagation velocities are calculated by the secant method, [15].

The threshold SIF was evaluated according to [15], where a threshold is assumed to be attained when the crack propagation velocity falls below 10^{-7} mm/cycle. In absence of valid data below this limit, an estimation of ΔK_{th} is made by a linear regression in a log-log plot of at least five points falling below 10^{-6} mm/cycle. In some cases the tests did not possess the requirement described above; ΔK_{th} was here estimated using the following procedure:

a) the last portion of the da/dN-ΔK data obtained in ΔK-decreasing tests was approximated with a power law
b) if points are available below 10^{-6} mm/cycle, the power law approximation is prolonged to intersect the line at 10^{-7} mm/cycle, taking it as an estimation of ΔK_{th}
c) if points are not available below 10^{-6} mm/cycle, the intersection with an horizontal line at 10^{-6} mm/cycle is taken as the corresponding ΔK as a less conservative estimation of ΔK_{th}.

4. RESULTS AND DISCUSSION

4.1 FCG resistance

In figure 5 the overall fatigue crack growth data for the two composites are reported. In the case of 6061/20p, the data are presented in the form of 95% prediction intervals, including both LT and TL orientations since the difference was not significant. Therefore, in the following analysis no distinction is made anymore between LT and TL orientations.

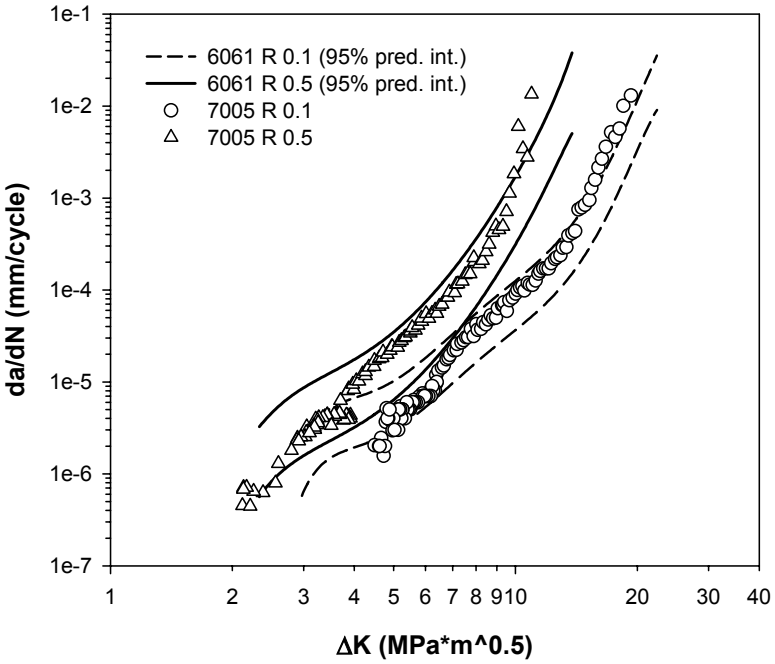

"**Fig. 5.** FCG resistance in AA6061/Al_2O_3/20p and AA7005/Al_2O_3/10p PMMCs"

The influence of *R*-ratio is instead clear and coherent with the behaviour of homogeneous materials: data are shifted to the left if load ratio increases, i.e. higher *R*-ratios correspond to higher propagation rates at the same applied ΔK. The two 6061/20p prediction intervals of tests at R=0.1 and R=0.5 overlap each other only partially and at the lower propagation rates.

FCG data relative to 7005/10p (round and triangular symbols) fall within the bounds traced for 6061/20p. Again the *R*-ratio play a significant role in FCG behaviour.

The parameters *C* and *m* of the Paris' law $da/dN=C(\Delta K)^m$ were extracted by fitting the experimental data within the range 10^{-5} to $3\cdot10^{-4}$ mm/cycle of the FCG rates in order to maximize the correlation coefficient. The threshold values were evaluated according to the procedure described previously. The results are summarized in Tab. 4. The exponent *m* is in line with data from literature for of SiC- and Al_2O_3-reinforced PMMCs [2, 7], and so does the estimated ΔK_{th} [5, 7].

In both alloys the *R*-ratio does not significantly affect the exponent *m* of the Paris' law, meaning that a different mechanism of propagation is not activated by a higher mean load. A higher dependence from *R*-ratio can be noticed in FCG rates parameter *C* and in ΔK_{th} values; it is to attribute to the premature crack closure, in which an active contribution is given by the presence of the particles. This is confirmed by the lower *C*-dependence from *R*-ratio in 7005/10p, where the reinforcement volume is 10%.

"**Table 4.** Parameters of the Paris' law of FCG behaviour and ΔK_{th} values"

Material	R	C	m	ΔK_{th} ($MPa\sqrt{m}$)
AA6061/Al_2O_3/20p	0.1	$7.88 \cdot 10^{-9}$	3.97	2.5(*)
	0.5	$1.04 \cdot 10^{-8}$	4.55	1.4
AA7005/Al_2O_3/10p	0.1	$6.14 \cdot 10^{-9}$	4.16	3.3(*)
	0.5	$1.74 \cdot 10^{-8}$	4.49	1.3

(*) estimated at 10^{-6}mm/cycle

The threshold values of 6061/20p and 7005/10p at R=0.5 (where crack closure is generally very low) are very similar, indicating that at very low growth rates and for an opened crack, the dependence from the particle volume becomes weak.

4.2 Fracture surfaces and crack profile roughness

SEM micrographs of fracture surfaces are reported in figure 6. The arrow indicates crack propagation direction. R-ratio is 0.5. Figure 6(a) shows the transcrystalline mechanism of failure in the 6061/20p in the near threshold regime. No clear instances of alumina particles are visible, as a result of the crack running inside the metal matrix. At higher applied stress intensity factor, ΔK = 13MPa$\sqrt{m}$, particle decohesion and fracture can be seen, figure 6(b). Highly deformed dimples around the particles are the trace of large plastic strain amount in the matrix, indicating a ductile failure mechanism.

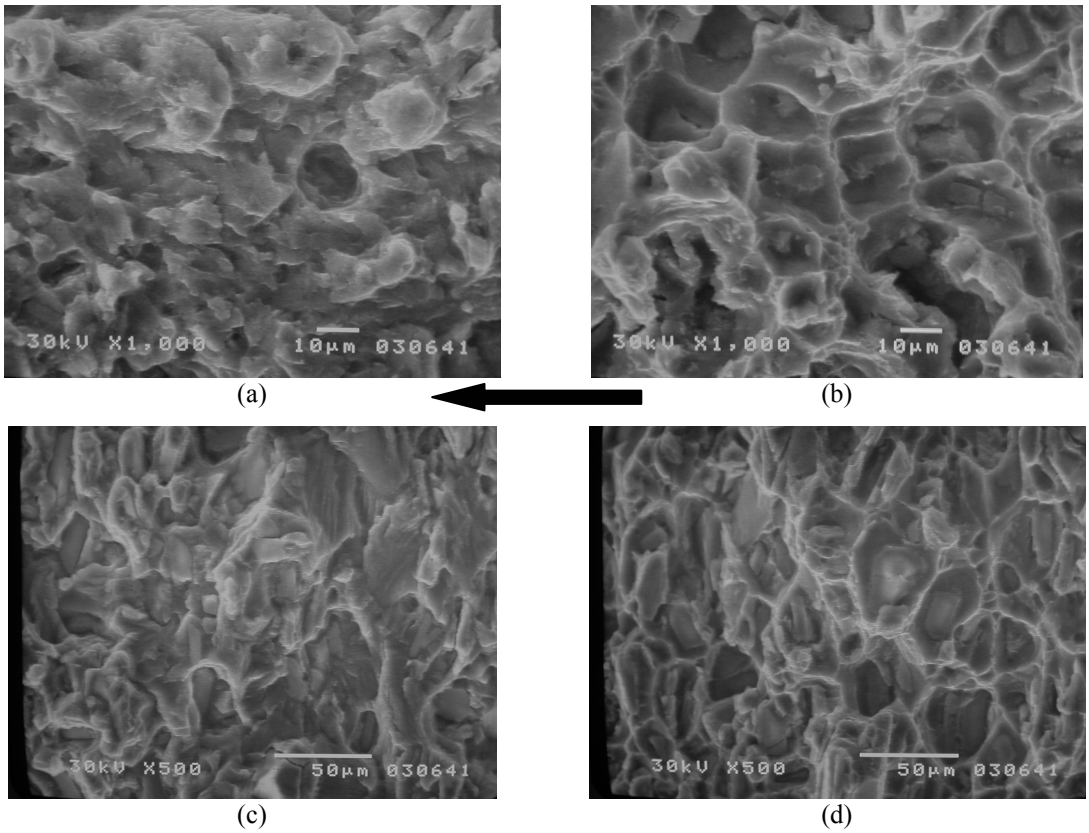

"**Fig. 6.** Fracture surfaces: (a) 6061/Al_2O_3/20p at R=0.5 in near threshold regime (ΔK = 5.1MPa$\sqrt{m}$) and (b) at ΔK = 13MPa$\sqrt{m}$; (c) 7005/Al_2O_3/10p at R=0.5, ΔK = 4.7MPa$\sqrt{m}$ and (d) at R=0.5 and ΔK = 11 MPa$\sqrt{m}$ "

Figures 6(c) and 6(d) show the equivalent conditions for the 7005/10p. At low ΔKs fracture appears always transcrystalline trough the matrix but there is a small extent of ridges and dimples, which were practically absent in the 6061 due to the higher content of particles. At higher loads, again a greater density of decohered and fractured particles indicates a ductile failure.

The roughness of crack profiles has been measured by superimposing a grid on SEM images taken at the specimen side. The number of intersection P_i between crack profile and grid lines of horizontal length L and vertical spacing y determines the roughness $R_v=(y/L)\Sigma_i P_i$. This simple technique can obviously give only a monodimensional estimate of roughness.

Results of roughness analysis are listed in Tab. 5, where also the effective length l_p of the profiles inside the measure window of wideness L are reported, in terms of l_p/L ratio.

"**Table 5.** Roughness and effective length of crack profile"

Material	R	R_v (μm) at low ΔK	R_v (μm) at high ΔK	l_p/L at low ΔK	l_p/L at high ΔK
AA6061/Al_2O_3/20p	0.1	0.22	0.51	1.14	1.33
	0.5	0.26	0.84	1.07	1.15
AA7005/Al_2O_3/10p	0.1	0.40	0.86	1.13	1.54
	0.5	0.46	0.93	-	-

It can be noticed that:

a) *coeteris paribus* the roughness R_v is higher in 7005 alloy (10% particle reinforcement)
b) roughness increases with ΔK in both reinforced alloys at each R-ratio
c) roughness slightly increases also with R-ratio if we fix the load
d) the adimensional length of crack profile l_p/L increases with ΔK in both the materials, in 6061 alloy it is higher at low R-ratio
e) differences between the two alloys in R_v are not found in l_p/L parameter also

The increase of roughness for increasing ΔK and load ratio is explained by the higher plastic deformation in the matrix. This is confirmed by the fact that in 7005/10p, where the matrix is more free to plastically deform due to the lower particle content, the roughness is generally higher.

The overall length of the crack path follows the same rend of the roughness at R=0.1, i.e. the lower the ΔK the lower the overall length. At R=0.5 (6061/20p only) instead, there is not a great difference between overall length at low and high ΔK, even though the roughness is significantly different. This fact may be explained considering that a higher plastic deformation occurs in the matrix at high ΔK, leaving a wake of ridges and dimples that increase roughness but whose contribution to the overall crack path length, which is inherently tortuos, is not significant.

4.3 Crack closure analysis

Roughness and particle-matrix interaction are in PMMCs the main causes of anticipated crack closure. Especially at low R-ratio and small cyclic load, roughness induced crack closure was found to be an important contribution to good FCG properties in particulate reinforced materials, [2, 3, 7]. In figure 7 a crack closure mechanism due to particle anticipated contact and mode II loading activation is clearly shown.

The analysis of (da/dN-ΔK) data in terms of effective ΔK_{eff} has been conducted with the models and techniques previously illustrated, in the near-threshold regime of FCG rate.

The results are reassumed in figure 8(a)-(d).

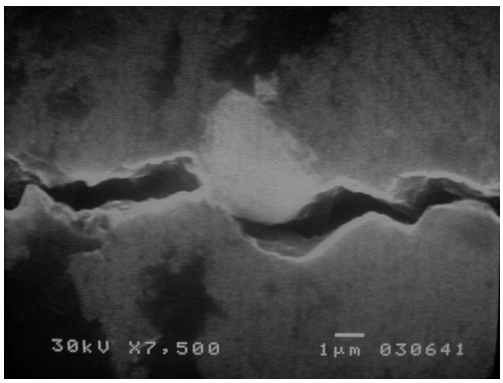

"**Fig. 7.** A particle causes the anticipated crack closure in 7005/Al_2O_3/10p"

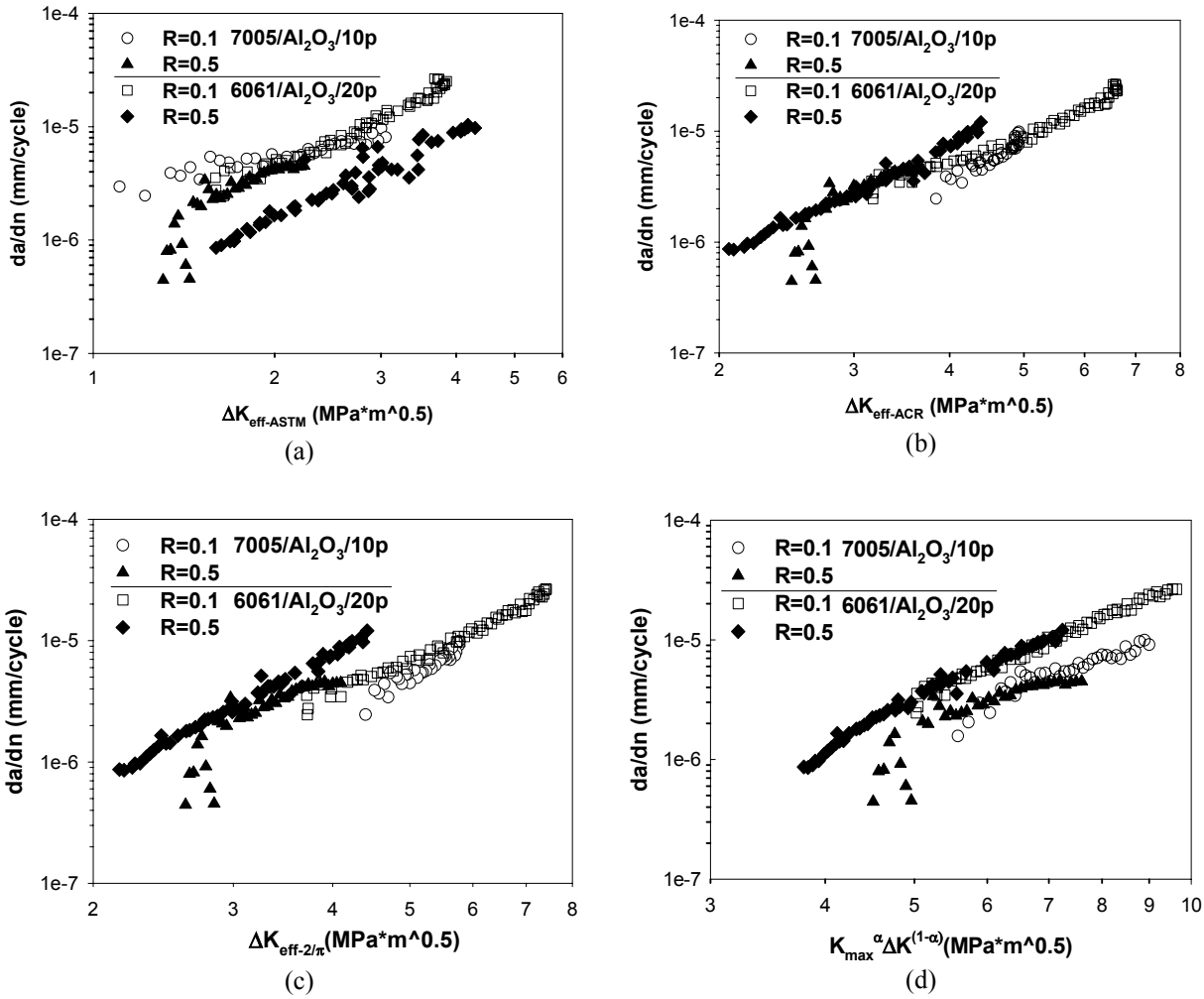

"**Fig. 8.** Near threshold FCG behaviour in terms of effective ΔK: (a) Elber traditional approach, [11]; (b) *ACR* technique, [12]; (c) 2/π model, [13]; (d) K_{max}-ΔK^+ model, [14]"

It is possibile to notice that the Elber's method, figure 8(a), gives good results in terms of data superposition, in the case of 7005 PMMC for crack velocities > $3\text{-}4\cdot10^{-6}$. At lower velocities the trend is instead diverging. In the case of 6061 PMMC, where closure mechanism is enhanced because of the higher reinforcement volume, it is even found that data at R=0.1 fall to the left of data at R=0.5. Thus, this method demonstrates not to be adequate to account for closure effect in this case.

With *ACR* technique, see figure 8(b), a good superposition of effective ΔK data points is obtained between the two materials at the same *R*-ratio. The best correlation of FCG rate vs. *R*-ratio is in the near-threshold regime.

Results very similar to *ACR* are found making use of the other partial closure method ($2/\pi$ model), figure 8(c). The double parameter model gives the best (da/dN-ΔK_{eff}) superposition, figure 8(d), with $\alpha = 0.7$ in eq. (4) for both the reinforced alloys. Besides, this model gives the best result in terms of reduction of data obtained at different *R*-ratios to a unique trend because it takes into account the influence K_{max}, which is of crucial importance in the case of brittle materials.

5. CONCLUSIONS

The fatigue crack growth behaviour of 6061-T6 and 7005-T6 aluminum alloy reinforced with 20% and 10% alumina particles has been characterized with standard crack propagation tests; fracture surfaces have been analysed at SEM, and FCG data in the near-threshold regime treated with crack closure arguments. The following main conclusions can be drawn:

- for 6061 PMMC the properties along LT and TL directions do not significantly differ
- FCG behaviour of 7005/10p are within the 95% prediction intervals of 6061/20p
- *R*-ratio highly influences the FCG resistance in PMMC as in homogeneous materials
- failure mechanism in boh PMMCs depends from the reinforcement volume percentage and from the load amount
- analysis of crack profile roughness can be an useful tools to correlate crack propagation and particle interaction mechanism to applied ΔK
- crack closure models applied to near-threshold data elaboration give unequal results of different quality. ASTM proposed technique demonstrates to be inadequate for this class of materials.

References

1. **Curran, G.**, *Materials World*, 20-21, Jan. 1998
2. **Clyne, T.W.** and **Withers, P.J.,** An Introduction to Metal Matrix Composites, Cambridge University Press, Cambridge, UK, 1995
3. **Shang, J.K.** and **Ritchie, R.O.,** *Acta Metall Mater,* 1989, **37**(88), 2267-2278
4. **Shang J.K., Yu, W., Ritchie** and **R.O.**, *Mater Sci Eng* 1988; A**102**, 181-192
5. **Lodgson, W.A.** and **Liaw, P.K.** (1986) *Eng Fract Mech* **24**, 737-751.
6. **Watt, D.F., Xu, X.Q., Lloyd** and **D.J.**, *Acta Mater,* 1996; **44**(2), 789-799
7. **Papakyriacou, M., Mayer, H.R., Tschegg-Stanzl, S.E.** and **Groschl, M.** *Fatigue Fract Eng M,* **18**, (1995), 477-487
8. **Kumai S., King, E.J.** and **Knott, J.F.,** *Fatigue Fract Eng M*, **13**, (1990), 477-487.
9. **Wang, Z.**, In *Key Engineering Materials* **104-107**, (1995), 765-790, Trans Tech Publications, Switzerland
10. **Liu, G.** and **Shang, J.K.,** *Acta Mater,* 44(1), (1996) 79-91
11. **Elber, W.**, *Eng Fract Mech*, (1970), 2:37-45
12. **Donald, J. K.,** *Int J Fatigue*, 19, (1997), S191/S195
13. **Paris, P. C., Tada, H.** and **Donald, J. K.,** *Int J Fatigue*, 21, (1999), S35/S46
14. **Kujawski, D.**, *Int J Fatigue,* **23**, (2001), S239/S246
15. **ASTM E647-00**, "Standard test method for Measurment of Fatigue Crack Growth Rates", *Annual Book of ASTM Standards - Vol. 3.01*, ASTM, USA
16. **Collini, L.** and **Pirondi, A.,** "Resistenza a frattura e propagazione di difetti di un composito particellato Al-Al_2O_3", In: Proc XXXI AIAS Nat Conf, (2002), Tipografia Benedettina, Parma, Italy (in italian)
17. **Shaw, W.J.D.** and **Zhao, W.,** *JTEVA* **22**, (1994), 512-516
18. **Nicoletto, G.** and **Pirondi, A.,** "Materialove inzinierstvo - Materials engineering Journal", **4**, Zilina University, Slovak Republic, (1997), 10-16